Food Hydrocolloids 155 (2024) 110228

Contents lists available at ScienceDirect

Food Hydrocolloids

journal homepage: www.elsevier.com/locate/foodhyd

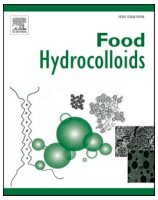

Interfacial and foaming properties of soluble lupin protein isolates: Effect of pH

Xingfa Ma , Mehdi Habibi , Leonard M.C. Sagis *

Laboratory of Physics and Physical Chemistry of Foods, Wageningen University, Bornse Weilanden 9, 6708 WG, Wageningen, the Netherlands

ARTICLE INFO

Keywords:
Lupin proteins
Interfacial rheology
Lissajous plots
General stress decomposition
Interfacial microstructure
Foaming properties

ABSTRACT

Lupins are rich in proteins (~40%) and fibers (~40%), and have been widely used for animal feed, but limitedly for human consumption due to the presence of alkaloids. Due to their high protein content, lupins have a high potential to be used as protein sources in diverse food manufacturing processes, including emulsion and foam stabilization. However, the interfacial properties of lupin protein isolates (LPI), especially their performance at different pH values, are not well understood so far. Here, we systematically investigated the air-water interfacial and foaming properties of the soluble fraction of LPI at pH 7.0, pH 6.0, pH 4.0, and pH 3.5. We observed that LPI at pH 4.0 (LPI-4) and pH 3.5 (LPI-3.5) adsorbed faster at the air-water interface than at pH 7.0 (LPI-7) and pH 6.0 (LPI-6) due to a smaller particle size and higher surface hydrophobicity of LPI-4 and LPI-3.5. This resulted in a higher foam overrun of LPI-4 and LPI-3.5 (300% and 331%, respectively). The air-water interfaces formed by LPI at different pH values were dramatically different in terms of interfacial structure and mechanical properties. LPI-4 and LPI-3.5 formed stiff and solid-like interfaces, leading to higher foam stability. In contrast, for LPI-7 there were clearly more protein aggregates at the interface, and this structure was weaker and less stretchable in response to shear and dilatational deformation, causing lower foam stability. LPI-6 also showed weaker air-water interfaces and thus formed less stable foams. Overall, LPI at acid pH (3.5 and 4) has a better performance in foam stabilization than at a pH close to neutral (6 and 7). Our results suggest that LPI can be potentially used as a plant-based clean-label additive in the production of foam-based food products in acidic environments.

1. Introduction

Lupins (*Lupinus* L., family Fabaceae), extensively cultivated in Australia and Mediterranean regions, are recently gaining increasing attention from food manufacturers due to their high protein contents and nutritional values (Lo, Kasapis, & Farahnaky, 2021; Noort, 2017, pp. 165–183; Shrestha, van't Hag, Haritos, & Dhital, 2021). Lupin seeds, such as *L. albus* L. (white lupin), consist of 34–49% of protein, 11.5–12.9% of fat, 30.5–36.9% of fibers, and 4.5% of carbohydrate (Bähr, Fechner, Hasenkopf, Mittermaier, & Jahreis, 2014; Martínez-Villaluenga, Frías, & Vidal-Valverde, 2006; Sujak, Kotlarz, & Strobel, 2006). Various techniques have been used to extract lupin proteins from lupin seeds, such as alkaline extraction followed by isoelectric precipitation, salt extraction, and ultrafiltration (Shrestha, et al., 2021). Lupin proteins mainly consist of four components, namely α-conglutin, β-conglutin, γ-conglutin, and δ-conglutin. Amongst these components, α- and β-conglutin are the main storage proteins, which account for 80–90% of the total protein content (Blagrove & Gillespie, 1975; Klupšaitė & Juodeikienė, 2015). Lupin proteins have shown promising functionality concerning foaming (El-Adawy, Rahma, El-Bedawey, & Gafar, 2001; Wäsche, Müller, & Knauf, 2001), emulsifying (El-Adawy, et al., 2001), and gelation properties (Bader, Oviedo, Pickardt, & Eisner, 2011; Rodríguez-Ambriz, Martínez-Ayala, Millán, & Davila-Ortiz, 2005; Vogelsang-O'Dwyer et al., 2020).

In this study, we mainly focus on aerated systems, also known as foams, that have been widely used in producing food products, such as cake, whipped cream, and mousse. The foaming properties of LPI (El-Adawy, et al., 2001; Vogelsang-O'Dwyer et al., 2020; Wong, Pitts, Jayasena, & Johnson, 2014) have been studied at neutral pH. It was reported that LPI prepared by micellization (i.e., a mixture of α-, β-, and γ-conglutin) and isoelectric precipitation (again a mixture) had a foaming capacity of 146% and 106%, respectively (El-Adawy, et al., 2001). In contrast, 1 % (w/w) of γ-conglutin (acid soluble protein fraction in LPI) showed a better foam capacity (FC) (around 394.4%) and foam stability (FS) (around 105 min of half-life time) (Wong, et al., 2014). Additionally, several studies have reported reduced FC and FS at

* Corresponding author.
E-mail address: leonard.sagis@wur.nl (L.M.C. Sagis).

https://doi.org/10.1016/j.foodhyd.2024.110228
Received 12 March 2024; Received in revised form 1 May 2024; Accepted 24 May 2024
Available online 25 May 2024

pH 4–6 compared to pH of 2 and 10 (Piornos, et al., 2015; Rodríguez-Ambriz, et al., 2005). However, most current studies only focus on the macroscopic foaming properties of lupin proteins, and the underlying foam formation and stabilizing mechanisms, especially their interfacial properties and microstructure of the air-water interface, are poorly understood. Besides, the application of protein source materials in food processing often involves adjustment of environmental factors (such as pH and temperature). In the pH regimes from 3 to 7, the intrinsic properties of LPI, such as protein solubility and particle size, vary greatly, which could potentially change their functionality. With this in mind, we aimed to investigate the effect of pH (3.5, 4, 6, and 7) on the interfacial properties of lupin proteins, and link these properties to their foaming properties at these pH values. With respect to the interfacial properties, we studied the adsorption kinetics, and the surface shear and dilatational properties, using both small and large amplitude oscillations. The dilatational results were analyzed with the general stress decomposition (GSD) (de Groot, Yang, & Sagis, 2023). The microstructure of the interfaces was imaged using atomic force microscopy on Langmuir-Blodgett films.

2. Materials and methods

2.1. Materials

Lupin protein seeds were purchased from Kamelur (Germany). Other chemicals (Sigma-Aldrich, USA) and materials for SDS-PAGE (Invitrogen Novex, ThermoFisher Scientific, USA) were used as received. All solutions in this study were made in Ultrapure water (MilliQ Purelab Ultra, Germany) unless stated otherwise.

2.2. Extraction of lupin protein

Lupin protein isolates (LPI) were extracted using a method described by Berghout, Boom, and Van der Goot (2014) with modifications. Briefly, lupin seeds were initially dehulled by a laboratory scale dehuller (Satake Corporation, Japan), followed by milling the lupin grits to full-fat flour using a multimill (Hosokawa-Alpine, Augsburg, Germany) with a ZPS50 configuration. The full-fat flour was further defatted three times using hexane in a 1:10 ratio (w/v) with continuous stirring for 2 h at room temperature. Subsequently, the defatted flour was dispersed in MiliQ water at a ratio of 1:10 ratio (w/v), and then the pH of the dispersions was adjusted to 9.0 using 1M NaOH. The mixture was centrifuged at 15,000 rpm for 10 min, followed by collecting supernatant. The pH of the supernatant was adjusted to 4.6 to precipitate proteins, for 90 min. Afterward, the protein precipitates were collected by centrifuging at 15,000 rpm for 5 min, followed by redispersing the protein pellets in MiliQ water and re-adjusting the pH to 7.2. The redispersed protein dispersions were dialyzed over 12 kDa cut-off membranes against MiliQ water at 4 °C for 72 h. The dialyzed protein suspensions were freeze-dried for further analysis.

2.3. Preparation of lupin protein solution

LPI solutions with 0.1% (w/w) concentration were prepared at pH 7.0 (denoted as LPI-7), pH 6.0 (denoted as LPI-6), pH 4.0 (denoted as LPI-4), and pH 3.5 (denoted as LPI-3.5), based on soluble protein contents, by dispersing protein powders in 20 mM pH 7.0 phosphate buffer, 20 mM pH 6.0 phosphate buffer, 20 mM pH 4.0 acetate buffer, and 20 mM pH 3.5 citrate buffer, respectively. All solutions were stirred for 4 h at room temperature and then stored at 4 °C overnight to allow complete hydration. Before further use, the protein solutions were passed through 0.45 μm syringe filters to remove insoluble materials.

2.4. Protein composition by sodium dodecyl sulfate-polyacrylamide gel electrophoresis

(SDS-PAGE).

Solutions of 0.1% (w/w) protein were prepared at pH 7.0, pH 6.0, pH 4.0, and pH 3.5 in corresponding buffers, and then mixed with NuPAGE LDS sample buffer, followed by heating at 70 °C for 10 min, and then loaded on a 12% (w/w) BisTris gel, next to a molecular marker of 10–200 kDa. These gels were run at 200 V for 30 min, before staining with SimplyBlue Safestain, and then scanned in a Biorad GS900 gel scanner.

2.5. Determination of particle size distribution and zeta potential

The particle size and zeta potential of 0.1 w/w% protein solutions were determined using dynamic light scattering in a Zetasizer Nano ZS (Malvern Instruments, UK). The refractive index of proteins and continuous phase was set at 1.45 and 1.33, respectively. All measurements were performed in triplicates at 25 °C.

2.6. Determination of protein solubility

Before measuring protein solubility, 1% (w/w) of lupin protein isolate solutions were prepared at pH 3–7 buffer for 4 h and kept overnight to allow for protein hydration, at 4 °C. Afterward, all protein solutions were passed through a 0.22 μm syringe filter to remove any insoluble particles before drying in an oven at 60 °C. The nitrogen content of the dried protein samples was measured using a Flash EA 1112 Series Dumas (Interscience, The Netherlands). A nitrogen conversion factor of 5.7 was used to calculate the protein content.

2.7. Determination of surface hydrophobicity

The surface hydrophobicity of proteins and mixtures was determined using 8-anilino-1-napthalenesulfonic acid ammonium salt (ANSA) as a fluorescence probe. Briefly, stock solutions (0.1 w/w%) were diluted to 0.002%, 0.004%, 0.006%, 0.008%, and 0.01% (w/w). Thereafter, 25 μL of 8 mM ANS solution was added in 3 mL solutions and was allowed to react for 1 h in the dark. The fluorescence intensity was measured using a fluorescence spectrometer (Shimadzu RF 6000 Fluorometer) at an excitation and emission wavelength of 390 nm and 470 nm, respectively. Buffer solutions (20 mM and pH 3.5–7.0) with ANSA were used as blanks. The initial slope of the fluorescence intensity against the protein concentration was determined to calculate surface hydrophobicity. All measurements were performed in duplicate.

2.8. Interfacial adsorption behavior

The interfacial adsorption behavior of lupin protein at the air-water interface was first studied by a Bubble Pressure Tensiometer (BPT) (BPT mobile, Krüss GmbH, Hamburg, Germany) for the short-time scale (10 ms-10s), followed by measurement with a Tracker Automated Droplet Tensiometer (ADT) (Teclis, France) for the long-timescale (1s–10800s). In short, BPT measures the pressure required to generate a small air bubble from a capillary (SH2510) at a different frequency within 15 ml of samples. In the ADT, a rising droplet of 15 mm^2 surface area was generated at the tip of a G16 needle and then equilibrated for 3 h. The surface tension was calculated by built-in software based on the shape of the droplet, captured by a camera, and subsequently fitted with the Young-Laplace equation. Surface pressure (Π) was calculated as $\Pi(t) = \gamma(t)\text{-}\gamma_0$, where $\gamma(t)$ is the surface tension at time t and γ_0 is the surface tension of the pure air-water interface. All samples were measured at least in triplicate at 20 °C.

2.9. Interfacial shear rheology

The air-water interface formed by lupin protein was subjected to shear deformations in an AR G2 rheometer (TA Instruments, USA) with a double wall ring (DWR) geometry, according to Shen, Peng, Sagis, & Landman, 2023. Briefly, 18.8 ml of protein solutions were first transferred into a Teflon double wall trough, before placing the DWR geometry at the air-water interface. After that, the interfaces were pre-sheared for 5 min and then left to equilibrate for 3 h, at rest. Subsequently, the interfaces were subjected to frequency sweeps and strain sweeps. In frequency sweeps, the frequency was increased from 0.01 Hz to 10 Hz at a fixed strain of 1%, followed by fitting the values of the surface shear storage modulus with a power law model ($G' \sim \omega^n$). In strain sweeps, the strains were increased from 0.1% to 100% at a fixed frequency of 0.1 Hz. The obtained torque was used to construct Lissajous plots. These experiments were conducted at 25 °C in triplicate.

2.10. Interfacial dilatational rheology

A rising droplet was created at the tip of a G16 needle, with a surface area of 15 mm^2, and aged for 3 h. The interface of this droplet was then subjected to sinusoidal oscillatory deformation in amplitude sweeps or frequency sweeps. The amplitude sweeps were conducted at an amplitude ranging from 5% to 50% at a fixed frequency of 0.02 Hz. Five cycles were applied for each amplitude, and the middle three cycles were used to create Lissajous curves of surface pressure vs. deformation $(A(t)-A_0)/A_0$, where $A(t)$ is the droplet area at time t and A_0 is the droplet area in the nondeformed state. The frequency sweeps were performed at a frequency of 0.005–0.1 Hz at a fixed amplitude of 3%. The frequency sweep results were fitted by a power law model ($E_d' \sim \omega^n$), where E_d' is the surface dilatational storage modulus and ω is the frequency (Hz).

2.11. Interfacial thickness measurement

The thickness of lupin protein stabilized air-water interfaces was measured by imaging nulling ellipsometer EP4 (Accurion, Germany) according to Shen, Yang, Nikiforidis, Mocking-Bode, and Sagis (2023). Briefly, a protein-stabilized interface was created by injecting 15 mL of protein solution into a Petri dish (60 mm diameter) and then allowing the interface to equilibrate for 3 h. Subsequently, an incident polarized laser light beam was used, and the intensity and polarization change of the reflected light beam were recorded at a wavelength from 499.8 to 793.8 nm over two zones, at an angle of incidence (AOI) of 50°. The output data were then analyzed by EP4Model v.3.6.1. software to calculate the interfacial thickness.

2.12. Preparation of Langmuir-Blodgett films

Lupin protein stabilized air-water interfacial films were deposited on mica sheets (Highest Grade V1 Mica, Ted Pella, USA) using a Langmuir trough (KSV NIMA/Biolin Scientific Oy, Finland). Briefly, the trough was filled with 20 mM buffer and a freshly cleaved mica sheet was immersed in the fluid. A total of 200 μL of 0.1% protein solution was injected at the bottom of the trough, followed by equilibration for 3 h. Afterward, the Teflon barriers were moved at a speed of 5 mm/min to compress the interfacial films until a surface pressure of 10 mN/m or 20 mN/m, while continuously monitoring the surface pressure by a Wilhelmy plate (platinum, perimeter 20 mm, height 10 mm). Next, the mica sheet was lifted vertically at a speed of 1 mm/min while keeping the surface pressure constant, to deposit the interfacial films onto the mica sheet. All films were prepared in duplicate and dried in a desiccator at room temperature.

2.13. AFM imaging and quantitative interfacial structure image analysis

The interfacial structures were observed with an atomic force microscope (AFM, NanoWizard® 4XP NanoScience, Bruker Nano GmbH, Germany). The peak force tapping mode was used to scan the film using a PEAKFORCE-HIRS-F-A cantilever (Bruker, USA) with a normal spring constant of 0.42 N/m and a normal tip radius of 1 nm. The scan area was set at 2×2 μm^2 with a set point of 0.5 nN and a line rate of 1.7 Hz. The image data were further analyzed using the Nanoscope Analysis v1.5 software (Bruker, USA). The protein network structure observed in the AFM images was analyzed using the Angiotool 64 software (National Cancer Institute, National Institute of Health, Maryland, USA), according to the previous studies (Bernklau, Lucas, Jekle, & Becker, 2016; Erturk, Bonilla, & Kokini, 2021; Zudaire, Gambardella, Kurcz, & Vermeren, 2011). Briefly, vessel area, vessel percentage area, junction density, average vessel length, end-point rate, branching rate, and mean lacunarity were calculated by the software to characterize the protein network. Image J was used to determine the pair correlation function (g(r)), which was used to investigate the heterogeneity of the film structure and determine the average domain size, according to Shen, Peng, Sagis, & Landman, 2023 and Munialo, van der Linden, Ako, and de Jongh (2015). Briefly, the raw images were initially converted to 8-bit grayscale images and then analyzed using the macro (radical distribution function) to perform the pair correlation function analysis.

2.14. Foamability and foam stability

Foamability and foam stability of lupin protein extracts were measured by whipping and gas sparging methods, respectively. In the whipping method, 15 ml of protein solution was transferred into a plastic cylinder tube (ø = 3.4 cm) and subsequently whipped at 2000 rpm for 2 min using a frother (Aerolatte, UK) that was driven by an overhead stirrer. The foam height and initial liquid height were measured by a ruler, and then the overrun (%) was calculated as overrun (%) = foam height (cm)/liquid height (cm) × 100%. In the gas sparging method, 40 mL of solution was transferred into a glass cylinder (ø = 25 mm), followed by sparging the protein solutions at a gas flow rate of 180 mL/min to a foam volume of 60 cm^3. The foam stability was assessed by the time required for half of the volume of the foam to decay (also called half-life time) based on the gas sparging method. The average air bubble size was measured by transferring the fresh foam between two transparent Plexiglas plates (10 × 10 cm) followed by gently squeezing the foam between two plates to a final fixed gap (between the two plates) of 0.26 mm. The morphology of the foam bubble was captured by taking high-resolution images of the 2D foam. The images were further analyzed by the software ImageJ to calculate the bubble size distribution after converting the 2D data of the area into 3D spherical volume. Examples of the 2D images are shown in the supplementary information (SI).

3. Results and discussion

3.1. Physicochemical properties of extracted lupin proteins

Electrophoresis (SDS-PAGE) was used to analyze the composition of the lupin protein solutions at pH 7.0, pH 6.0, pH 4.0, and pH 3.5. Under non-reducing conditions, all bands (L1, L3, L5, and L7) are mainly distributed at 50–55 kDa, 35–45 kDa, 24 kDa, and 12–15 kDa, which corresponded to α-conglutin (11S), β-conglutin (7S), γ-conglutin (7S), and δ-conglutin (2S), respectively (Duranti, Consonni, Magni, Sessa, & Scarafoni, 2008; Mane, Johnson, Duranti, Pareek, & Utikar, 2018). Under reducing conditions (L2, L4, L6, and L8), the intensity of these main bands was reduced and split into two other bands (heavy chains and light chains). To quantitatively analyze the effect of pH on the protein compositions of lupin protein, the intensity of SDS-PAGE bands in Fig. 1A was further analyzed by ImageJ. From the quantitative result in Fig. 1B, it appears that the distribution of protein subunits at different pH values was not significantly changed.

The particle size of proteins is a key parameter influencing their

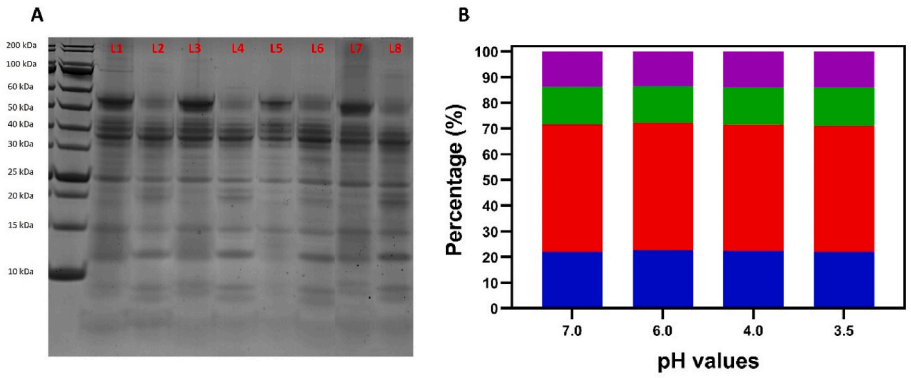

Fig. 1. (A) SDS-PAGE scan gel under reducing (L2, L4, L6, and L8) and non-reducing (L1, L3, L5, and L7) conditions with a molecular marker and lupin protein isolate (LPI) at pH 7.0 (L1, L2), pH 6.0 (L3, L4), pH 4.0 (L5, L6), and pH 3.5 (L7, L8). (B) Quantitative analysis of SDS-PAGE bands (α-conglutin (11S) (■), β-conglutin (■), γ-conglutin (7S) (■), and δ-conglutin (■)) of LPI solutions under non-reducing conditions at pH 7.0, pH 6.0, pH 4.0, and pH 3.5.

interfacial properties, including their diffusion rates towards the air-water interface and interfacial stability. The particle size distribution of soluble LPI fractions (S-LPI) at different pH values is shown in Fig. 2A. The soluble fraction of LPI at pH 7.0 clearly showed bimodal distributions, where the first peak was between 20 and 70 nm with a maximum at 32.3 nm, while another peak was between 80 and 420 nm with a maximum at 197.6 nm, indicating the existence of globulin aggregates at neutral pH. When the pH was reduced from 6.0 to 3.5, the particle size distribution of S-LPI became a monomodal distribution and the peak reduced from 15.2 to 11.2 nm. In this process the zeta potential (Fig. 2B) changed from negative at pH 6 and 7, to positive at pH 3.5 and 4. The charge neutralization during this transition may cause the precipitation of the large protein aggregates (~197.6 nm) existing in the LPI at pH 7 (in view of the reduced protein solubility at the intermediate pH values (Fig. 2C)). Another possible reason for the smaller particle size of LPI at acidic pH compared to pH 7 might be attributed to the dissociation of protein subunits at acidic pH that frequently occurs in plant proteins (Tang, Roos, & Miao, 2023).

Changes in surface hydrophobicity (H_0) reflect protein conformational changes (protein unfolding or exposure of protein hydrophobic groups on the surface) during the pH shifting process (Mohan, Ramachandran, & Sankar, 2006), and may potentially affect the interfacial properties of proteins (Chang, Tu, Ghosh, & Nickerson, 2015). As shown in Fig. 2D, the surface hydrophobicity of LPI slightly reduced from pH 7.0 to 6.0 but dramatically increased at pH 3.5 and 4.0. The lower surface hydrophobicity at pH 6.0 might be because the protein has a higher tendency to aggregate at a pH close to the isoelectric point, resulting in buried hydrophobic groups which are less accessible to ANS (Jarpa-Parra, et al., 2015; Jingqi Yang, Liu, Zeng, & Chen, 2018). The relatively higher surface hydrophobicity of LPI at pH 3.5 and 4.0 could be explained by the dissociation of protein subunits at pH 3.5 and 4.0, which exposes more hydrophobic groups (Ge, et al., 2021; J. Li et al.,

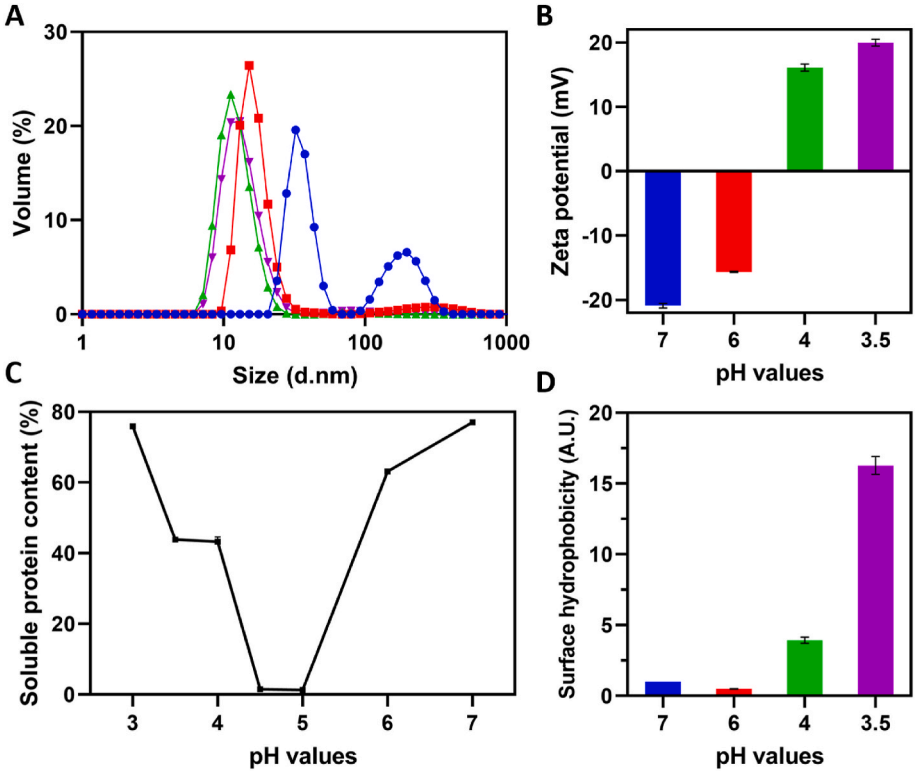

Fig. 2. (A) The volume-based particle size distribution of LPI at pH 7.0 (—●—), pH 6.0 (—■—), pH 4.0 (—▲—), and pH 3.5 (—▼—). (B) Zeta potential as a function of pH of 0.1 % (w/w) LPI. (C) Soluble protein content (%) of LPI as a function of pH. (D) Relative surface hydrophobicity of LPI at pH 7.0, pH 6.0, pH 4.0, and pH 3.5.

2020). Similar results were also reported by Jarpa-Parra, et al. (2015), where lentil proteins showed a higher surface hydrophobicity at pH 3.0 than at pH 5.0 and 7.0.

3.2. Adsorption behavior of lupin protein towards air-water interface

The interfacial adsorption behavior of lupin protein at pH 7.0 (LPI-7), pH 6.0 (LPI-6), pH 4.0 (LPI-4), and pH 3.5 (LPI-3.5) was studied in both the sub-second (10-10,000 ms) and long-time (1–10,800 s) regimes. To investigate the early stages of adsorption in the sub-second regime, and determine whether it is diffusion-controlled or energy barrier-controlled, we rescaled the time axis of the curves in Fig. 3A, such that the surface pressure of all samples starts to increase at dimensionless time 1. This resulted in a single master curve (Fig. 3C), and the scaling factor is equal to the adsorption lag time of each LPI sample. The surface pressure results suggested that LPI-4 and LPI-3.5 diffused faster towards the interface than LPI-7 and LPI-6, due to the smaller particle size of LPI-4 and LPI-3.5. We further plotted the scaling factor (lag time) against particle size (from Fig. 2A) to determine the relationship between these two factors. The adsorption lag time of LPI-3.5 was shorter (0.19 ± 0.01 s) than that of LPI-4 (0.36 ± 0.02 s), although LPI-3.5 had a slightly larger particle size (15.9 ± 0.4 nm) than LPI-4 (13.9 ± 0.4 nm). This implies that the adsorption is not purely diffusion-controlled. Previous experiments have shown that the zeta potential of the pure air-water interface is negatively charged, and this was attributed to hydroxide ions (OH^-) more preferentially adsorbing to the interface over H^+ ions, resulting in an excess amount of OH^- ions near the air-water interface (Beattie, Djerdjev, & Warr, 2009; C. Li & Somasundaran, 1991; Manciu & Ruckenstein, 2012; Takahashi, 2005). As shown in Fig. 2B, LPI-3.5 was slightly more positively charged than LPI-4.0. The larger net positive charges of LPI-3.5 may result in stronger attractive forces between the positively charged protein molecules and negatively charged air-water interface, which may in turn increase the adsorption rate of LPI-3.5 towards the air-water interface. Besides, protein surface hydrophobicity was previously related to the adsorption process of proteins to the air-water interface (Bender, 1991; Bergfreund, Bertsch, & Fischer, 2021; de Jongh et al., 2004; Schwenke, 1998, pp. 1–50). The energy barriers for protein adsorption were found to be lower for proteins with higher surface hydrophobicity due to the strong affinity with hydrophobic interfaces (Narsimhan & Uraizee, 1992; Wierenga, Meinders, Egmond, Voragen, & de Jongh, 2003). LPI-3.5 had a significantly higher surface hydrophobicity than LPI-4.0 (Fig. 2D), which may reduce the energy barriers for adsorption and thus increase its adsorption rate to the air-water interface. Similar results were reported by Baszkin, Boissonnade, Kamyshny, and Magdassi (2001), where a sample with more exposed hydrophobicity of human immunoglobulin G adsorbed faster to the air-water interface than a native one.

Regarding the long-term adsorption process (Fig. 3B), the surface pressure of LPI-3.5 and LPI-4.0 reaches a relatively lower value of 24.7 mN/m and 25.8 mN/m, respectively, after 10,800 s, compared to LPI-6 and LPI-7 with an equilibrium surface pressure of 28.2 mN/m and 29.4 mN/m, respectively. The different equilibrium surface pressures among these LPI samples might be caused by protein surface activity, protein conformational changes, and protein in-plane interactions. In the next section, we will further characterize the interfacial properties by measuring the interfacial rheology and imaging the interfacial structure.

3.3. Interfacial shear rheology of lupin protein stabilized air-water interface

3.3.1. Frequency sweeps

After 3h of adsorption, the S-LPI stabilized air-water interfaces were subjected to shear deformation in both frequency sweeps and strain sweeps. In frequency sweeps, all interfaces showed that the storage

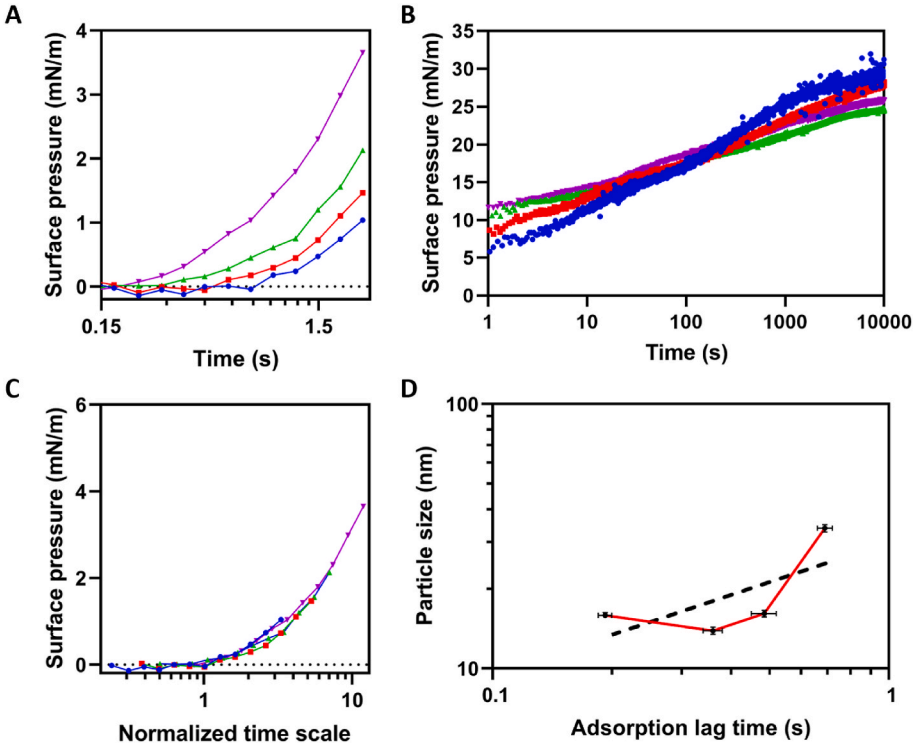

Fig. 3. Surface pressure of LPI at pH 7.0 (●), pH 6.0 (■), pH 4.0 (▲), and pH 3.5 (▼), as a function of time within the sub-second regime measured by bubble pressure tensiometer (BPT) (A) and within the long-time regime measured by automatic drop tensiometer (ADT) (B). Note that the values for plot A and plot B at 1 s were not the same, due to the use of different techniques, but the trends in plot A and B are comparable. (C) Superposition of adsorption curves of LPI at pH 7.0, pH 6.0, pH 4.0, and pH 3.5 measured by BPT (Fig. 3A). (D) The average particle size depicted from Fig. 2A versus adsorption lag time as determined from Fig. 3C for LPI at pH 7.0, 6.0, 4.0, and 3.5. The dashed line in Fig. 3D is the power law scaling with an exponent of 0.5, which would indicate diffusion-controlled adsorption.

modulus (G′) is larger than the loss modulus (G″) (Fig. 4A), indicating a viscoelastic solid-like behavior of interface with predominately elastic behavior. The plots for G′ displayed power law behavior for most of the frequency range, except for frequencies above 2 Hz, where a sudden upswing can be seen in LPI-6 and LPI-3.5, and a small decrease in LPI-7 and LPI-4, which we attribute to inertial effects. We fitted the G′ curves in the linear part of Fig. 4A with the power-law model ($G' \sim \omega^n$) (Fig. 4B), and the interfaces showed n-values of around 0.1–0.2, behavior suggesting a wide spectrum of relaxation times and the formation of soft disordered solid-like interfacial structures (Sollich, 1998; Winter & Mours, 1999).

3.3.2. Strain sweeps

The surface shear modulus as a function of strain (0.1–100%) of LPI-7, LPI-6, LPI-4, and LPI-3.5 is shown in Fig. 5A. In the strain sweeps, the G′ modulus starts with a constant value until a critical strain, which represents the end of the linear viscoelastic (LVE) regime. The extent of the LVE regime represents the stretchability of the interfaces under the applied strain before the microstructure of the interfaces is disrupted, and the response becomes nonlinear. The LPI-6 showed the longest LVE regime of 3.2%, while LPI-7, LPI-4, and LPI-3.5 had an approximately equal value of 1.6%, indicating the formation of a more stretchable air-water interface by LPI-6. In the LVE regimes, LPI-4 and LPI-3.5 showed a higher G′ value (0.063 and 0.050 N/m, respectively) than LPI-7 and LPI-6 (0.008 and 0.026 N/m, respectively), indicating LPI-4 and LPI-3.5 formed stiffer interfaces than LPI-7 and LPI-6. The higher interfacial stiffness of LPI-4 and LPI-3.5 could be related to their higher surface hydrophobicity that increased attractive interactions between proteins at the interface. In the non-linear viscoelastic (NLVE) regimes, the G′ values start to reduce until a crossover point, where the value of G′ drops below the value of G‘‘. LPI-6 had the highest crossover point (63.1%) compared with LPI-7 (15.9%), LPI-4 (50.2%), and LPI-3.5 (56.3%), indicating LPI-6 stabilized interfaces retain solid-like behavior over a wider range of strains than LPI-7, LPI-4, and LPI-3.5. Additionally, LPI-7 stabilized interfaces showed an overshoot in the G″ curve between strains of 2% and 10%. This response is called type III nonlinear behavior, while the gradual decrease in both G’ and G” observed for the three other samples is classified as type I behavior. Type III behavior is frequently found in particle network systems, and attributed to a process in which partially disrupted networks form new clusters by particle collisions, resulting in temporary shear-thickening behavior, before disrupting these clusters again at higher strains (Hyun, Kim, Ahn, & Lee, 2002). For a more quantitative analysis of the differences in nonlinear behavior we constructed Lissajous curves of time-dependent torque versus strain, and these are discussed in the next section.

3.3.3. Lissajous plots in interfacial shear rheology

To reveal more information about interfacial shear rheology in the LVE and NLVE regimes, normalized Lissajous plots were constructed (Fig. 5B). In the LVE regime (0.5%), all plots showed narrow and elliptical shapes with straight decomposed elastic torque curves, indicating linear viscoelastic behavior, dominated by the elastic contribution. In the NLVE regime (16%–100%), all Lissajous plots become wider and change to a rhomboidal shape with inverted sigmoidal decomposed elastic torque curves, indicating the disruption of the interfacial structure increased the viscous contributions to the total torque response. The Lissajous plots of LPI-6, LPI-4, and LPI-3.5 were less distorted at 30% strain than that of LPI-7, and their decomposed elastic curves were relatively straighter. At 100%, all Lissajous plots become almost rectangular, indicating their interfacial structure was mostly disrupted at 100%, and the interfaces were showing plastic behavior. The slopes of the decomposed elastic curves of LPI-6, LPI-4, and LPI-3.5 were steeper than that of LPI-7, suggesting more residual elasticity of the former interfaces even at 100% strain.

The energy dissipation ratio (Φ) was calculated to quantitatively analyze the linear/non-linear behaviors in the Lissajous plots (Fig. 5C). In the LVE regime, the Φ of all interfaces is less than 0.2, indicating a predominant elastic behavior. In the NLVE regime, the Φ of LPI-7 stabilized interfaces dramatically increases between a strain of 2%–40%, and finally keeps constant at 0.74 until a strain of 100%. By contrast, the Φ of LPI-6, LPI-4, and LPI-3.5 was much lower than LPI-7 at strains up to about 10% and then showed a more gradual increase in Φ. LPI-6, LPI-4, and LPI-3.5 clearly formed a disordered viscoelastic solid-like air-water interface that was stiffer than the LPI-7 in small shear deformation, and these interfaces were also more stretchable than LPI-7 in response to large deformations.

3.4. Interfacial dilatational rheology of lupin protein stabilized air-water interface

3.4.1. Frequency sweeps

The LPI-stabilized air-water interface was further subjected to dilatational deformations in frequency and amplitude sweeps. In the frequency sweeps, the dilatational elastic modulus was again fitted with a power law model ($E_d' \sim \omega^n$), and the n values of all interfaces were between 0.08 and 0.15 (Fig. 6A), which is significantly lower than 0.5. These results indicate that all interfaces (LPI-7, LPI-6, LPI-4, and LPI-3.5) had low exchangeability of protein between bulk and interface (Lucassen & Van Den Tempel, 1972) and confirmed our observations from the surface shear experiments that the LPI is forming soft disordered solid-like interfaces at all pH values.

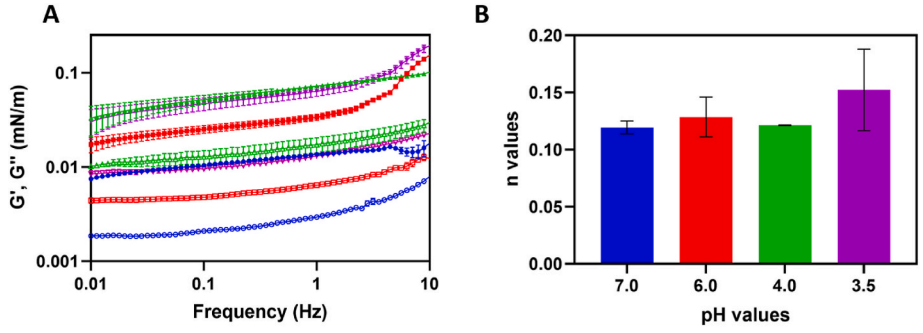

Fig. 4. Interfacial shear modulus (G′ and G″) of LPI at pH 7.0 (—●— and —○—), pH 6.0 (—■— and —□—), pH 4.0 (—▲— and —△—), and pH 3.5 (—▼— and —▽—) as a function of frequency and at a fixed strain of 1%. (B) The power law fitting exponent n was calculated from the interfacial shear frequency sweep at 1% strain for LPI at pH 7.0, pH 6.0, pH 4.0, and pH 3.5, using only frequencies in the range of 0.01–1 Hz.

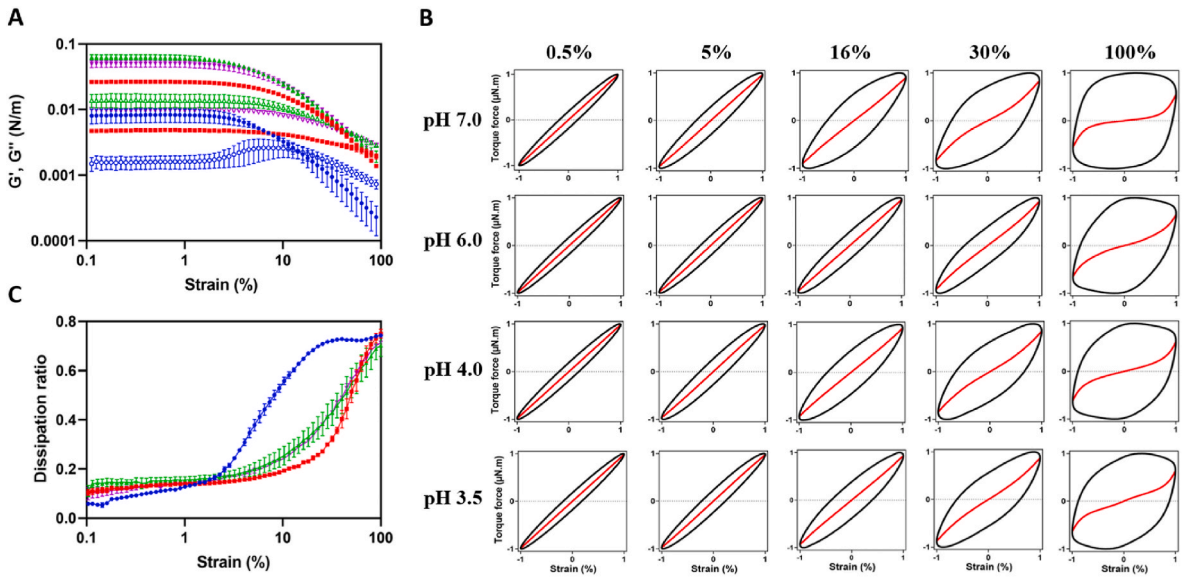

Fig. 5. (A) The surface shear modulus (G′, G″) of LPI at pH 7.0 (—●— and —○—), pH 6.0 (—■— and —□—), pH 4.0 (—▲— and —△—), and pH 3.5 (—▼— and —▽—), as a function of strain. (B) Normalized Lissajous plots of torque as a function of the applied strain for lupin protein at pH 7.0, pH 6.0, pH 4.0, and pH 3.5. The red curve in the interior of the loop denotes the elastic contribution to the total torque. (C) The dissipation ratio as a function of strain of interfaces stabilized by LPI at pH 7.0 (—●—), pH 6.0 (—■—), pH 4.0 (—▲—), and pH 3.5 (—▼—).

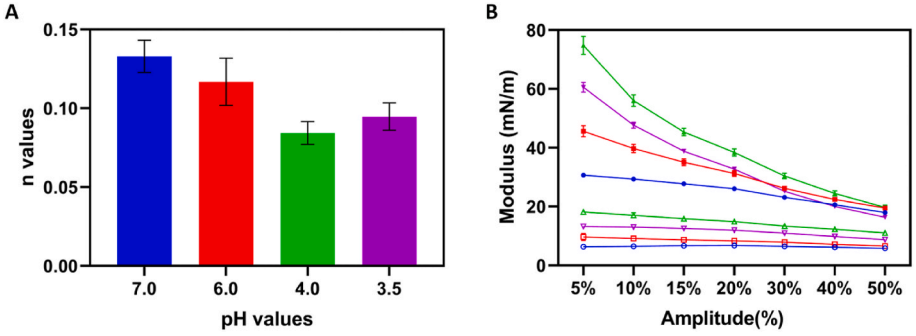

Fig. 6. (A) The values of power-law exponent n were obtained from the interfacial dilatational frequency sweeps at a fixed strain of 3% for LPI at pH 7.0, pH 6.0, pH 4.0, and pH 3.5. (B) Interfacial dilatational storage (E_d') and loss (E_d'') modulus as a function of deformation amplitude for lupin protein pH 7.0 (—●— and —○—), pH 6.0 (—■— and —□—), pH 4.0 (—▲— and —△—), and pH 3.5 (—▼— and —▽—). The closed symbols represent the storage modulus, and the open symbols represent the loss modulus.

3.4.2. *Amplitude sweeps*

The dilatational moduli (E_d' and E_d'') of LPI as a function of amplitude at different pH levels is shown in Fig. 6B. The storage modulus of all interfaces significantly reduced from values between 30.7 and 74.8 mN/m at 5% to 18.0–19.7 mN/m at 50%, indicating the disruption of interfacial structures with increased amplitude. At lower amplitude (5%), LPI-4 had the highest E_d' values of 74.8 mN/m, followed by LPI-3.5 (60.5 mN/m) and LPI-6 (45.6 mN/m), while LPI-7 had the lowest E_d' values of 30.7 mN/m, indicating LPI-4 formed the stiffest interface with strong in-plane interactions, while LPI-7 formed the weakest interface.

3.4.3. *Lissajous plots for interfacial dilatational rheology*

In the calculation of the dilatational modulus in Fig. 6, only the intensity and phase of the first harmonic of the Fourier transform of the surface pressure are used, while the contributions from higher harmonics are ignored (Ewoldt, Hosoi, & McKinley, 2008). When higher-order harmonics are present in the total response, the first harmonic-based modulus may not provide accurate information. Therefore, we constructed Lissajous plots to analyze the non-linear rheology of LPI stabilized interfaces at different pH (Fig. 7).

At 5–10% amplitude, all plots showed ellipsoidal and narrow shapes, indicating predominantly elastic behavior. For LPI-4 and LPI-3.5, their plots were more titled towards the vertical axis than LPI-7 and LPI-6, suggesting the formation of stiffer interfaces. When the amplitudes increased, the plots became asymmetric and wider, indicating an increased non-linear response and increased viscous contributions. At 50% deformation, the surface pressure increased markedly at the start of extension (bottom left corner of the plots), implying a high initial interfacial stiffness, followed by a gradual reduction of the slope of the Lissajous plot due to the reduced interfacial density and disruption of the interfacial structure. This phenomenon is called strain-softening. The

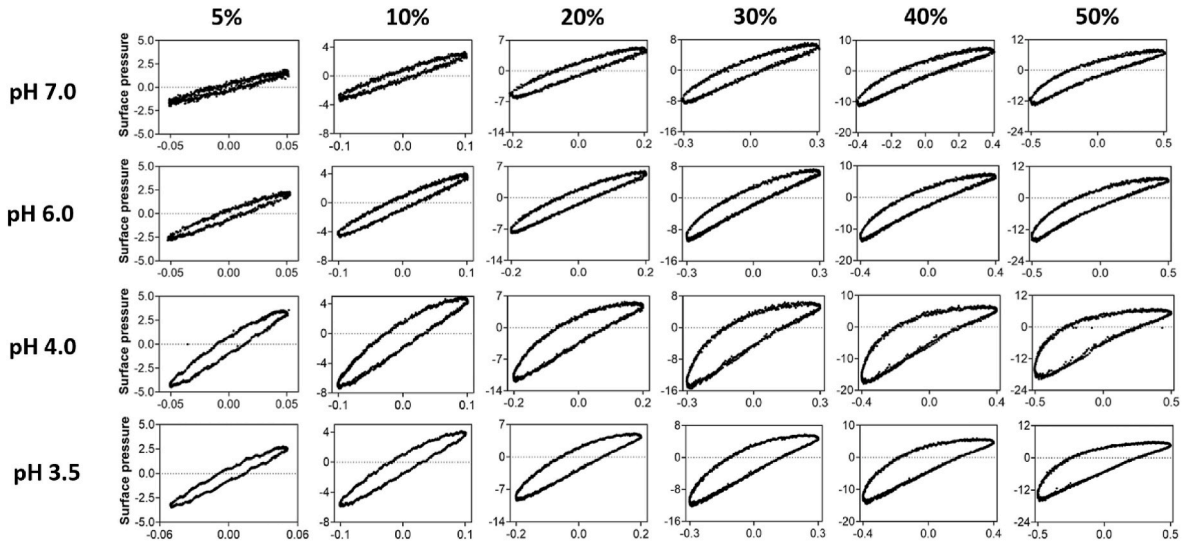

Fig. 7. Lissajous plots of surface pressure as a function of deformation for lupin protein at pH 7.0, pH 6.0, pH 4.0, and pH 3.5. For clarity, one plot is shown for each sample from the amplitude sweeps, but the three replicate results were comparable.

opposite phenomenon appears in the compression stage, where strain-hardening occurs due to the increased surface density and jamming of the interfacial structure. When comparing the non-linearities of LPI at different pH, we found that LPI-4 had the most pronounced strain-softening and strain-hardening compared with LPI-7, LPI-6, and LPI-3.5. However, this non-linear behavior could be from both network disruption and surface density changes. In this next section, we will further use general stress decomposition (GSD) to separate these two responses.

3.4.4. *General stress decomposition of Lissajous plots*

To better understand the nonlinearities at large deformation, we further applied a general stress decomposition to split the overall surface stress into a term containing only odd harmonics, and a term consisting of only even harmonics. The odd harmonics are related to the change of interfacial microstructure and consist of an elastic and a viscous contribution (denoted as τ_1 and τ_2, respectively). The even harmonics describe the contributions to the surface stress due to changes in surface density, which can also be split into an elastic and dissipative contribution (denoted as τ_3 and τ_4, respectively) (de Groot, et al., 2023).

For all interfaces at 50% amplitude, the odd harmonics ($\tau_1 + \tau_2$) display a slightly distorted ellipsoidal loop, particularly at pH 4, where the loop has taken on a rhomboidal shape (Fig. 8B and C). The secant modulus, $E_{\tau 1L}$, is the slope of the curve connecting the origin with the maximum in τ_1 and is a measure of the interfacial stiffness. All interfaces show a decrease of $E_{\tau 1L}$ with increasing strain amplitude (Fig. 9A), indicating the disruption of the interfacial microstructure with increased amplitude. We see that LPI-4 and LPI-3.5 formed a stiffer interface than LPI-6 and LPI-7, as indicated by their higher values of $E_{\tau 1L}$. LPI-7 has the lowest value for $E_{\tau 1L}$ and displays only a minor decrease of that modulus with increasing strain. This indicates that at this pH, LPI does not form a strong network, in line with the results of the surface shear experiments, where this sample also had the lowest value for G'. Regarding the viscous contributions (τ_2) to the odd harmonics, LPI-4 and LPI-3.5 had a significantly wider τ_2 loop than LPI-6 and LPI-7. The total area of the enclosed loop of τ_2 is calculated as $U_{d\tau 2}$ (Fig. 9D), which indicates the energy dissipation per unit area, per cycle. LPI-4 shows relatively higher values and a steeper increase of $U_{d\tau 2}$ with increasing amplitude, indicating stronger in-plane interactions that require more energy to disrupt the interfacial structure. In line with the previous results, LPI-7 has the lowest values for $U_{d\tau 2}$, confirming that this sample is not forming a strong network at the air-water interface.

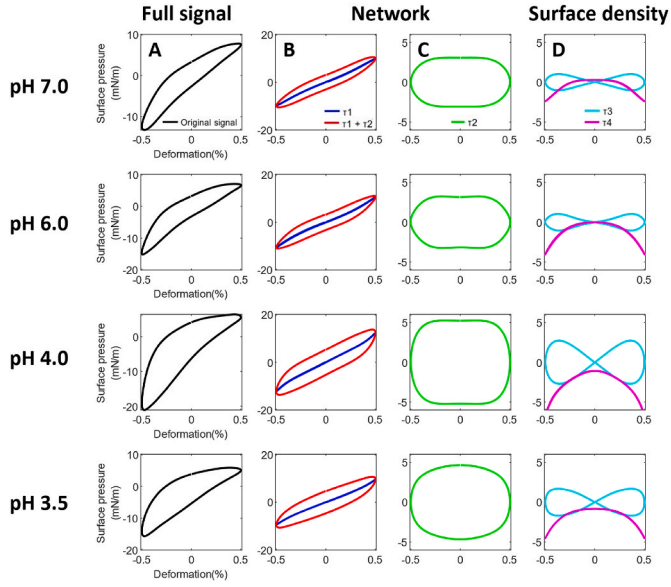

Fig. 8. Decomposed Lissajous plots of LPI at pH 7.0, pH 6.0, pH 4.0, and pH 3.5, from top to bottom at an oscillation amplitude of 50%. The fitted full signal is shown in black (—), τ_1 is shown in dark blue (—), $\tau_1 + \tau_2$ is shown in red (—), τ_2 is shown in green (—), τ_3 is shown in cyan (—), and τ_4 is shown in magenta (—).

The contributions of even harmonics ($\tau_3 + \tau_4$) to the total stress of LPI-stabilized interfaces are shown in Fig. 8D. The elastic part of even harmonics (τ_4) is characterized as a single lemniscate shape and is a measure for the energy storage from the surface pressure-area work exerted on the interface resulting from changes in surface density. The extent of τ_4 is quantitatively characterized by a secant modulus ($E_{\tau 4}$). At large deformation (>10%), LPI-4 had a more negative $E_{\tau 4}$ value compared with LPI-3.5, LPI-6, and LPI-7, suggesting surface density changes had more important contributions to the total surface stress in the LPI-4 stabilized interface. This may indicate there is limited bulk-interface exchange and strong in-plane interactions in the densely packed LPI-4 interface. The vertical shift of the τ_4 curve (its magnitude is given by γ_s) is a measure for the extent that the system is driven out of the equilibrium due to the applied deformations. All interfaces show a

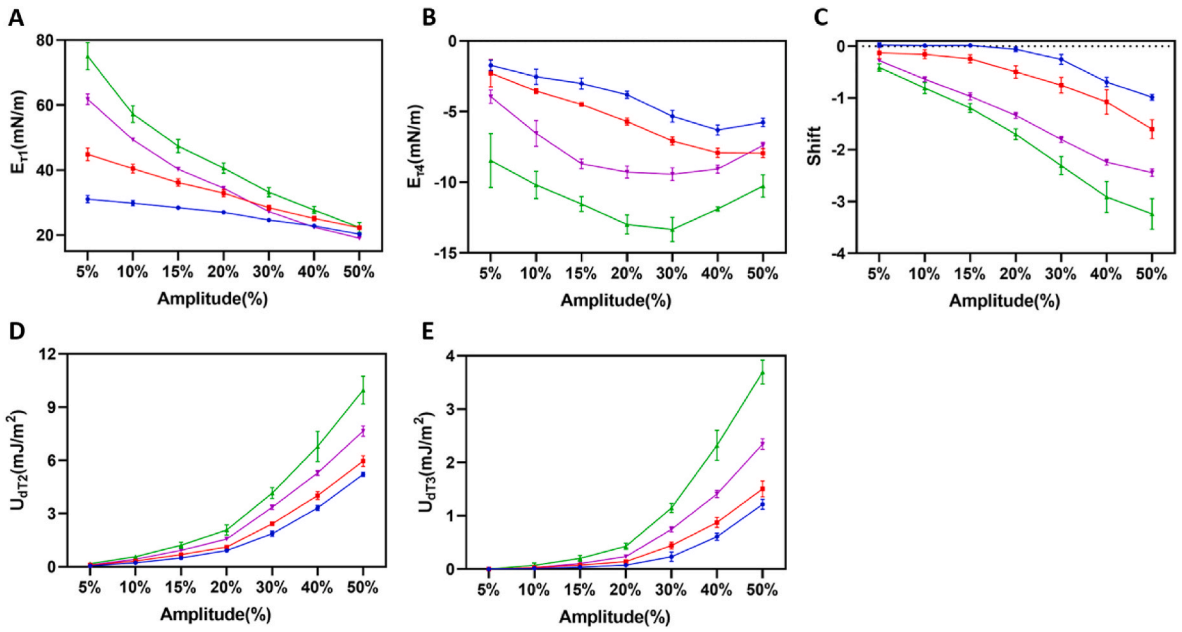

Fig. 9. The secant modulus of τ_1 (A), modulus of τ_4 (B), vertical shift (γ_s) of τ_4 (C), dissipated energy of τ_2 (D), dissipated energy of τ_3 (E) as a function of amplitude (%) for LPI at pH 7.0 (—●—), pH 6.0 (—■—), pH 4.0 (—▲—), and pH 3.5 (—▼—).

trend of γ_s decreasing to a more negative value as the increased amplitude. Among these interfaces, LPI-4 had a more negative γ_s value at 50% amplitude than LPI-3.5, LPI-6, and LPI-7, indicating the oscillations occur around a nonequilibrium state far from the equilibrium surface pressure-area isotherm. The highly negative value for $E_{\tau 4}$ and significant vertical shift for LPI-4 indicate the interface formed at this condition is dense and has reduced in-plane mobility of the proteins, leading to slow in-plane relaxation, and thus the LPI-4 stabilized interface cannot restore itself quickly to an equilibrium state at zero deformation. The energy dissipation per unit area per cycle associated with the τ_3 curve ($U_{d\tau 3}$) was also calculated and shown in Fig. 9E. LPI-4 stabilized interface clearly showed a wider τ_3 loop (Fig. 8D) and a higher value of $U_{d\tau 3}$ than LPI-3.5, LPI-6, and LPI-7 (Fig. 9E), again indicating a higher density and therefore higher viscous contribution.

Overall, the interfaces stabilized with LPI at an acidic environment (LPI-4 and LPI-3.5) were stiffer and denser than LPI at a pH close to neutral (LPI-6 and LPI-7), possibly due to the smaller particle size and higher surface hydrophobicity of LPI at acidic pH. The fact that LPI-4 forms a stiffer interface than LPI-3.5 could be due to the slightly lower charge of LPI at pH 4, which results in lower electrostatic repulsion between the proteins. This can lead to a denser packing and the formation of a stronger network. To check these hypotheses, we investigated the structure of the air-water interface by creating LB films, which were imaged with AFM. These images are discussed in the next section.

3.5. Interfacial structure of LPI at the air-water interface

To reveal the interfacial microstructure of the LPI-stabilized air-water interface, we prepared Langmuir-Blodgett films at a surface pressure of 10 mN/m and 20 mN/m, and then observed these films using AFM to study their topographical features (Fig. 10).

In the AFM images, the protein-rich regions are visible as bright areas, and the interfaces formed with LPI at all pH values clearly showed heterogeneous structures. At a surface pressure of 10 mN, LPI-7 appears to form larger and more aggregated clusters than LPI-6, LPI-4, and LPI-3.5. As expected, all interfaces at a surface pressure of 20 mN were denser than the ones at 10 mN. LPI-7 seems to form a more heterogeneous structure at the surface pressure of 20 mN compared with LPI at other pH values. This higher degree of heterogeneity was confirmed by its higher value for the maximum in g(r) (1.20) and significantly larger domain size (78.1 nm) based on pair correlation function analysis (Fig. S1 and Table S2, in the supplementary material) and higher lacunarity (0.0223) obtained from the protein network analysis (Fig. 11F). The AFM images show that at a surface pressure of 20 mN, LPI-7 formed thicker and larger protein aggregates with sizes of up to 254.4 nm (Fig. S1E), than LPI at other pH values. The thicker interface of LPI-7 was

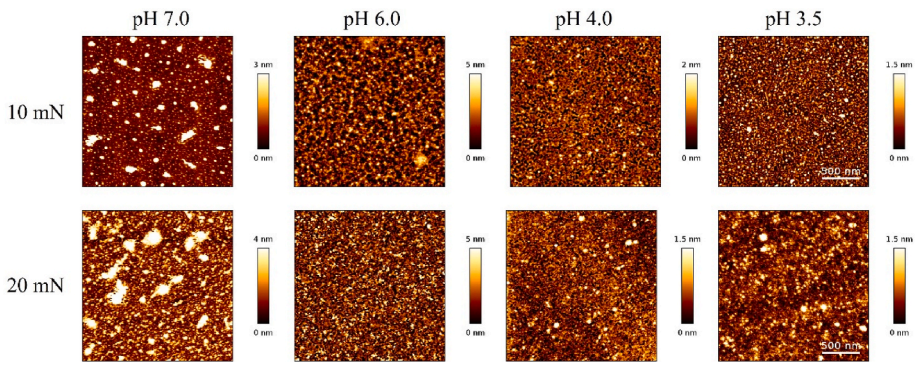

Fig. 10. AFM images of Langmuir-Blodgett films prepared from LPI at pH 7.0, pH 6.0, pH 4.0, and pH 3.5. The surface pressure applied during film preparation and the scan scale used during AFM imaging were indicated on the left side. The relative height (color bar) of the film was indicated on the right side.

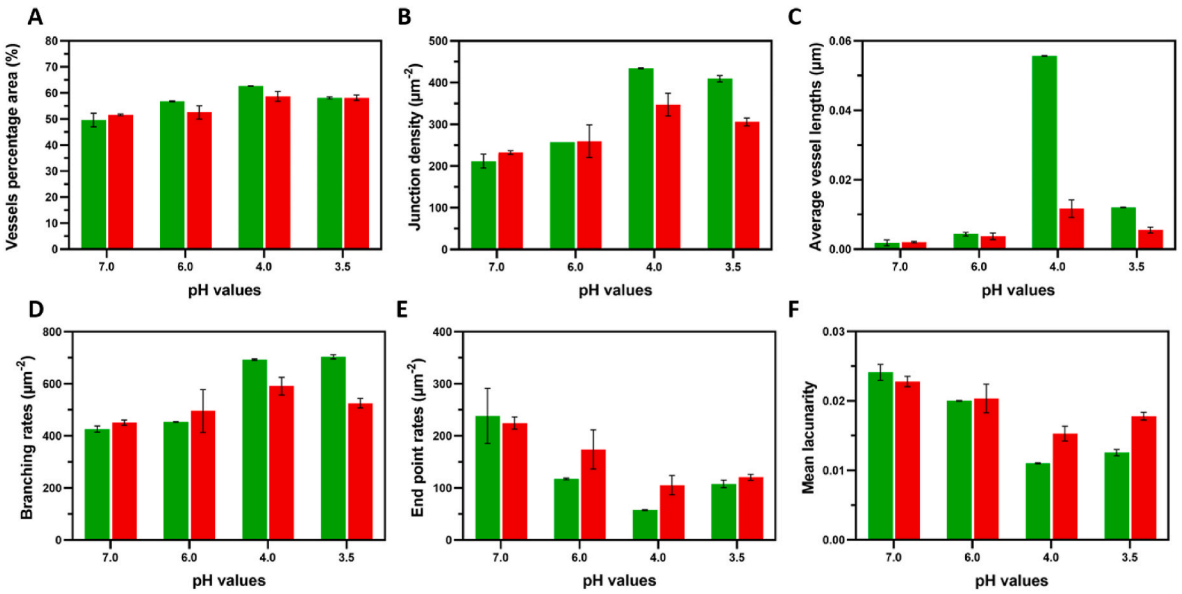

Fig. 11. Protein network variables (vessels percentage area (A), junction density (B), average vessel length (C), branching rates (D), endpoint rates (E), and mean lacunarity (F)) determined by AngioTool for LPI at pH 7.0, pH 6.0, pH 4.0, and pH 3.5, and at a surface pressure of 10 mN/m ( ) and 20 mN/m ( ).

also confirmed by ellipsometry measurements, which showed that LPI-7 had the highest thickness of 8.5 nm (Table S1). We further quantified the interfacial structure using the AngioTool 64 software, and observed that at both surface pressures, LPI-4 and LPI-3.5 have a higher network area, higher junction density, longer protein threads, higher branching rate, and lower end-point rate than LPI-7 and LPI-6 (Fig. 11A–E). These results indicate that LPI-4 and LPI-3.5 tend to form a dense and more fine-stranded air-water interface than LPI-7 and LPI-6.

Overall, LPI-7 tends to form coarser air-water interfaces with larger aggregates and lower connectivity between those aggregates, which in turn can explain the lower interfacial stiffness in response to dilatation and shear deformations than LPI-4 and LPI-3.5. The more homogeneous structure with higher connectivity for LPI-4 and LPI-3.5 explains the higher stiffness in surface shear and dilatation. The strong contribution from the odd harmonics in dilatation would suggest that at acidic pH LPI forms a 2d gel at the interface. The image analysis of the AFM images for LPI-7, combined with the low values for $E_{\tau 1L}$, and the minor dependence of that modulus on strain amplitude, suggest the formation of either a very weak gel or a soft glass-like structure of the interface. The slightly higher stiffness for LPI-4 compared to LPI-3.5, is in line with the former's higher vessel percentage area, higher junction density, longer average vessel length, higher branching rate, lower end point rate, and lower lacunarity. So as we mentioned before, this structure is indeed somewhat denser and more homogeneous than the structure of LPI-3.5. And

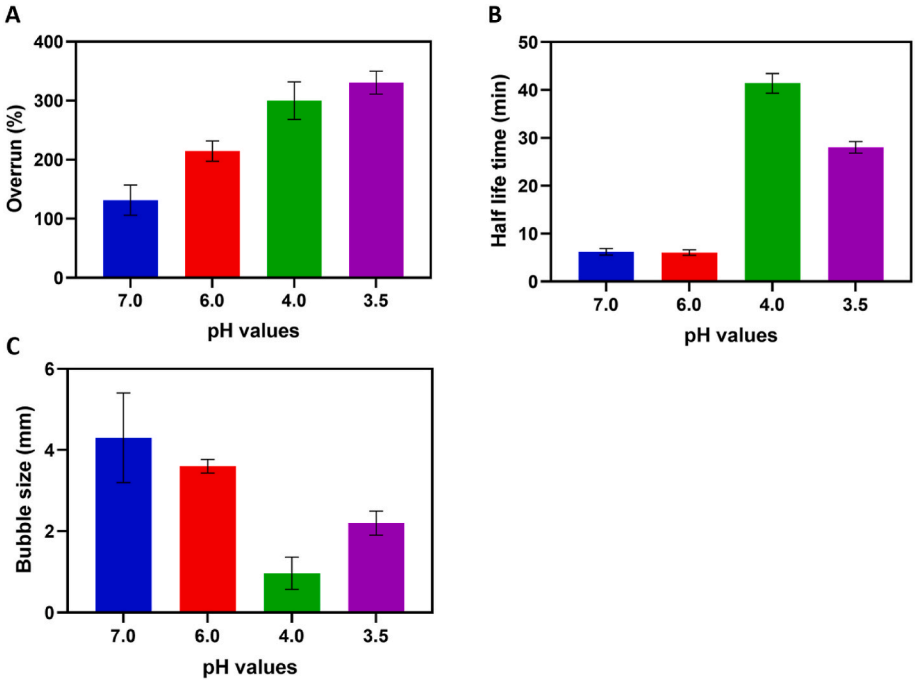

Fig. 12. The overrun (A), volume half-life time (B), and average bubble size (C) of foams stabilized by soluble fraction of lupin proteins at pH 7.0, pH 6.0, pH 4.0, and pH 3.5.

this is most likely related to the lower charge of the protein at pH 4.

3.6. Foaming properties of lupin proteins at different pH

To monitor the foamability and foam stability of interfaces stabilized by lupin proteins, liquid foams were produced by both whipping and N_2 gas sparging. To characterize these properties, overrun and half-life time (the time required for half of the volume of foam to decay) were determined and results are shown in Fig. 12A and B, respectively.

Both LPI-4 and LPI-3.5 showed a higher foam overrun of 300% and 331%, respectively, while LPI-6 and LPI-7 displayed relatively lower foam overrun of 215% and 131%, respectively. These results suggested good foamability of LPI at acidic pH, which was comparable with those of WPI (228%) (J. Yang, Gimenez-Ribes, He, Habibi, & Sagis, 2023), rapeseed protein concentrate (372–384%) (Jack Yang et al., 2021), and lentil protein (around 280%) (Shen, Peng, Sagis, & Landman, 2023). The foamability of proteins was affected by both (1) the adsorption rate towards the air-water interface and (2) the interfacial stability of the air bubbles against shear deformation during the whipping process. In sections 3.2 and 3.3, we observed that LPI-4 and LPI-3.5 diffused faster towards the air-water interface and had higher interfacial shear stiffness than LPI-7 and LPI-6, which resulted in higher foamability of LPI-4 and LPI-3.5.

LPI-4 stabilized foams showed the highest half-life time of 41.4 ± 2.1 min, followed by LPI-3.5 with a half-life time of 28.0 ± 1.2 min, while LPI-7 and LPI-6 displayed the lowest half-life time of 6.2 min (Fig. 12B). The foam stability was previously reported to be affected by interfacial stiffness (mainly from dilatational rheology) (Martin, Grolle, Bos, Stuart, & van Vliet, 2002; Murray, 2002; Prins, 1999). As indicated in sections 3.3 and 3.4, LPI-4 formed the stiffest air-water interface, which resulted in a significantly higher foam half-life time than LPI at other pH values. Additionally, the bubble size of LPI-4 stabilized foams was much smaller compared with those of LPI-7 and LPI-6. The larger air bubble size also contributes to less stable foams being formed with LPI-7 and LPI-6.

In short, LPI at acid pH (3.5 and 4) had better foamability and foam stability than LPI at a pH close to a neutral environment (6 and 7). As mentioned in section 3.1, the protein composition of LPI was not significantly changed at various pH conditions, but LPI-4 and LPI-3.5 had significantly smaller particle sizes than LPI-7 and LPI-6. The smaller particle sizes of LPI-4 and LPI-3.5 formed a stiffer and more compact air-water interface, which increased foamability and foam stability.

4. Conclusions

In this study, we systematically investigated the interfacial rheology and interfacial structure of air-water interfaces stabilized by the soluble fraction of lupin protein isolates at different pH values. We also showed how these properties can be related to the foaming properties of lupin protein isolates. Soluble LPI in acidic environments (pH 3.5 and 4) diffused faster towards the air-water interface than at a close to neutral pH (6 and 7), due to their smaller particle size and higher surface hydrophobicity, leading to a higher foamability. After adsorption at the air-water interface, LPI formed different interfacial structures with significantly different mechanical responses to dilatational and shear deformation, depending on pH. LPI at acidic pH tends to form a more homogeneous and compact air-water interface with a more fine-stranded network structure and thus forms a stiffer and more gel-like interface, which results in higher foam stability. In comparison, LPI at pH 7.0 tends to form a heterogeneous structure with large protein aggregates at the air-water interface, which results in reduced interfacial stiffness and foam stability.

This study revealed the interfacial properties of lupin protein at different pH environments, with respect to their interfacial adsorption behavior and interfacial shear and dilatational rheology. Overall, lupin protein at acid pH showed promising foaming properties, which may promote their application as a clean-label functional ingredient in the food industry. However, their poor solubility (around 44%) at acidic pH may be unsustainable for food mass production. Future studies should consider strategies, such as electrostatic complexation with polysaccharides, ultrasound, and enzymatic modification, to increase the solubility of lupin proteins at acidic pH. Although the interfacial structure of LPI at different pH values was characterized by AFM with Langmuir-Blodgett films, the interactions responsible for the formation of the disordered solid structure we observed, are still poorly understood. Therefore, in-situ techniques, such as synchrotron scattering techniques (e.g., GISAXS, WAXS, and synchrotron SAXS) and fluorescence micro-spectroscopy techniques (e.g., STORM, PALM, and FRAP), could be used to provide more information about the interfacial structure of LPI at the air-water interface.

CRediT authorship contribution statement

Xingfa Ma: Writing – original draft, Visualization, Validation, Methodology, Investigation, Conceptualization. **Mehdi Habibi:** Writing – review & editing, Supervision, Methodology, Conceptualization. **Leonard M.C. Sagis:** Writing – review & editing, Supervision, Methodology, Conceptualization.

Declaration of competing interest

The authors have declared that no competing interest exists.

Data availability

Data will be made available on request.

Acknowledgments

The authors have declared that no competing interest exists. X. Ma acknowledges the funding from China Scholarship Council (CSC NO. 202207940007).

Appendix A. Supplementary data

Supplementary data to this article can be found online at https://doi.org/10.1016/j.foodhyd.2024.110228.

References

Bader, S., Oviedo, J. P., Pickardt, C., & Eisner, P. (2011). Influence of different organic solvents on the functional and sensory properties of lupin (Lupinus angustifolius L.) proteins. *LWT-Food Science & Technology, 44*(6), 1396–1404.

Bähr, M., Fechner, A., Hasenkopf, K., Mittermaier, S., & Jahreis, G. (2014). Chemical composition of dehulled seeds of selected lupin cultivars in comparison to pea and soya bean. *LWT - Food Science and Technology, 59*(1), 587–590.

Baszkin, A., Boissonnade, M., Kamyshny, A., & Magdassi, S. (2001). Native and hydrophobically modified human immunoglobulin G at the air/water interface: Sequential and competitive adsorption. *Journal of Colloid and Interface Science, 239*(1), 1–9.

Beattie, J. K., Djerdjev, A. M., & Warr, G. G. (2009). The surface of neat water is basic. *Faraday Discussions, 141*, 31–39.

Bender, M. (1991). *Interfacial phenomena in biological systems* (Vol. 39). CRC Press.

Bergfreund, J., Bertsch, P., & Fischer, P. (2021). Adsorption of proteins to fluid interfaces: Role of the hydrophobic subphase. *Journal of Colloid and Interface Science, 584*, 411–417.

Berghout, J., Boom, R., & Van der Goot, A. (2014). The potential of aqueous fractionation of lupin seeds for high-protein foods. *Food Chemistry, 159*, 64–70.

Bernklau, I., Lucas, L., Jekle, M., & Becker, T. (2016). Protein network analysis—a new approach for quantifying wheat dough microstructure. *Food Research International, 89*, 812–819.

Blagrove, R., & Gillespie, J. (1975). Isolation, purification and characterization of the seed globulins of Lupinus angustifolius. *Functional Plant Biology, 2*(1), 13–27.

Chang, C., Tu, S., Ghosh, S., & Nickerson, M. (2015). Effect of pH on the interrelationships between the physicochemical, interfacial and emulsifying properties for pea, soy, lentil and canola protein isolates. *Food Research International, 77*, 360–367.

de Groot, A., Yang, J., & Sagis, L. M. (2023). Surface stress decomposition in large amplitude oscillatory interfacial dilatation of complex interfaces. *Journal of Colloid and Interface Science, 638*, 569–581.
de Jongh, H. H., Kosters, H. A., Kudryashova, E., Meinders, M. B., Trofimova, D., & Wierenga, P. A. (2004). Protein adsorption at air–water interfaces: A combination of details. *Biopolymers: Original Research on Biomolecules, 74*(1-2), 131–135.
Duranti, M., Consonni, A., Magni, C., Sessa, F., & Scarafoni, A. (2008). The major proteins of lupin seed: Characterisation and molecular properties for use as functional and nutraceutical ingredients. *Trends in Food Science & Technology, 19*(12), 624–633.
El-Adawy, T., Rahma, E., El-Bedawey, A., & Gafar, A. (2001). Nutritional potential and functional properties of sweet and bitter lupin seed protein isolates. *Food Chemistry, 74*(4), 455–462.
Erturk, M. Y., Bonilla, J. C., & Kokini, J. (2021). Relationship of non-linear rheological properties and quantitative network analysis parameters as a function of increasingly large amplitude deformations in non-fat, low-fat and high-fat yogurt products. *Food Hydrocolloids, 111*, Article 106194.
Ewoldt, R. H., Hosoi, A., & McKinley, G. H. (2008). New measures for characterizing nonlinear viscoelasticity in large amplitude oscillatory shear. *Journal of Rheology, 52*(6), 1427–1458.
Ge, J., Sun, C.-X., Mata, A., Corke, H., Gan, R.-Y., & Fang, Y. (2021). Physicochemical and pH-dependent functional properties of proteins isolated from eight traditional Chinese beans. *Food Hydrocolloids, 112*, Article 106288.
Hyun, K., Kim, S. H., Ahn, K. H., & Lee, S. J. (2002). Large amplitude oscillatory shear as a way to classify the complex fluids. *Journal of Non-Newtonian Fluid Mechanics, 107*(1–3), 51–65. Journal of Non-Newtonian Fluid Mechanics, 107(1), 51-65.
Jarpa-Parra, M., Bamdad, F., Tian, Z., Zeng, H., Temelli, F., & Chen, L. (2015). Impact of pH on molecular structure and surface properties of lentil legumin-like protein and its application as foam stabilizer. *Colloids and Surfaces B: Biointerfaces, 132*, 45–53.
Klupšaitė, D., & Juodeikienė, G. (2015). Legume: Composition, protein extraction and functional properties. *A Review Chemical Technology, 66*(1), 5–12.
Li, C., & Somasundaran, P. (1991). Reversal of bubble charge in multivalent inorganic salt solutions—effect of magnesium. *Journal of Colloid and Interface Science, 146*(1), 215–218.
Li, J., Wu, M., Wang, Y., Li, K., Du, J., & Bai, Y. (2020). Effect of pH-shifting treatment on structural and heat induced gel properties of peanut protein isolate. *Food Chemistry, 325*, Article 126921.
Lo, B., Kasapis, S., & Farahnaky, A. (2021). Lupin protein: Isolation and techno-functional properties, a review. *Food Hydrocolloids, 112*, 106318.
Lucassen, J., & Van Den Tempel, M. (1972). Dynamic measurements of dilational properties of a liquid interface. *Chemical Engineering Science, 27*(6), 1283–1291.
Manciu, M., & Ruckenstein, E. (2012). Ions near the air/water interface: I. Compatibility of zeta potential and surface tension experiments. *Colloids and Surfaces A: Physicochemical and Engineering Aspects, 400*, 27–35.
Mane, S. P., Johnson, S. K., Duranti, M., Pareek, V. K., & Utikar, R. P. (2018). Lupin seed γ-conglutin: Extraction and purification methods-A review. *Trends in Food Science & Technology, 73*, 1–11.
Martin, A. H., Grolle, K., Bos, M. A., Stuart, M. A. C., & van Vliet, T. (2002). Network forming properties of various proteins adsorbed at the air/water interface in relation to foam stability. *Journal of Colloid and Interface Science, 254*(1), 175–183.
Martínez-Villaluenga, C., Frías, J., & Vidal-Valverde, C. (2006). Functional lupin seeds (Lupinus albus L. and Lupinus luteus L.) after extraction of α-galactosides. *Food Chemistry, 98*(2), 291–299.
Mohan, M., Ramachandran, D., & Sankar, T. (2006). Functional properties of Rohu (Labeo rohita) proteins during iced storage. *Food Research International, 39*(8), 847–854.
Munialo, C. D., van der Linden, E., Ako, K., & de Jongh, H. H. (2015). Quantitative analysis of the network structure that underlines the transitioning in mechanical responses of pea protein gels. *Food Hydrocolloids, 49*, 104–117.
Murray, B. S. (2002). Interfacial rheology of food emulsifiers and proteins. *Current Opinion in Colloid & Interface Science, 7*(5–6), 426–431.
Narsimhan, G., & Uraizee, F. (1992). Kinetics of adsorption of globular proteins at an air-water interface. *Biotechnology Progress, 8*(3), 187–196.
Noort, M. V. D. (2017). *Lupin: An important protein and nutrient source. Sustainable protein sources*. Academic Press. https://doi.org/10.1016/B978-0-12-802778-3.00010-X.
Piornos, J. A., Burgos-Díaz, C., Ogura, T., Morales, E., Rubilar, M., Maureira-Butler, I., et al. (2015). Functional and physicochemical properties of a protein isolate from AluProt-CGNA: A novel protein-rich lupin variety (Lupinus luteus). *Food Research International, 76*, 719–724.
Prins, A. (1999). Stagnant surface behaviour and its effect on foam and film stability. *Colloids and Surfaces A: Physicochemical and Engineering Aspects, 149*(1–3), 467–473.
Rodríguez-Ambriz, S., Martínez-Ayala, A., Millán, F., & Davila-Ortiz, G. (2005). Composition and functional properties of Lupinus campestris protein isolates. *Plant Foods for Human Nutrition, 60*, 99–107.
Schwenke, K. (1998). Proteins: Some principles of classification and structure, *Vol. 7. Studies in interface science*. Elsevier.
Shen, P., Peng, J., Sagis, L. M., & Landman, J. (2023). Air-water interface properties and foam stabilization by mildly extracted lentil protein. *Food Hydrocolloids, 147*, 109342.
Shen, P., Yang, J., Nikiforidis, C. V., Mocking-Bode, H. C., & Sagis, L. M. (2023). Cruciferin versus napin–Air-water interface and foam stabilizing properties of rapeseed storage proteins. *Food Hydrocolloids, 136*, Article 108300.
Shrestha, S., van't Hag, L., Haritos, V. S., & Dhital, S. (2021). Lupin proteins: Structure, isolation and application. *Trends in Food Science & Technology, 116*, 928–939.
Sollich, P. (1998). Rheological constitutive equation for a model of soft glassy materials. *Physical Review A, 58*(1), 738.
Sujak, A., Kotlarz, A., & Strobel, W. (2006). Compositional and nutritional evaluation of several lupin seeds. *Food Chemistry, 98*(4), 711–719.
Takahashi, M. (2005). ζ potential of microbubbles in aqueous solutions: Electrical properties of the gas− water interface. *The Journal of Physical Chemistry B, 109*(46), 21858–21864.
Tang, Q., Roos, Y. H., & Miao, S. (2023). Plant protein versus dairy proteins: A pH-dependency investigation on their structure and functional properties. *Foods, 12*(2), 368.
Vogelsang-O'Dwyer, M., Bez, J., Petersen, I. L., Joehnke, M. S., Detzel, A., Busch, M., et al. (2020). Techno-functional, nutritional and environmental performance of protein isolates from blue lupin and white lupin. *Foods, 9*(2), 230.
Wäsche, A., Müller, K., & Knauf, U. (2001). New processing of lupin protein isolates and functional properties. *Nahrung, 45*(6), 393–395.
Wierenga, P. A., Meinders, M. B., Egmond, M. R., Voragen, F. A., & de Jongh, H. H. (2003). Protein exposed hydrophobicity reduces the kinetic barrier for adsorption of ovalbumin to the air− water interface. *Langmuir, 19*(21), 8964–8970.
Winter, H. H., & Mours, M. (1999). Rheology of polymers near liquid-solid transitions. *Neutron spin echo spectroscopy viscoelasticity rheology* (pp. 165–234).
Wong, A., Pitts, K., Jayasena, V., & Johnson, S. (2014). Isolation and foaming functionality of acid-soluble protein from lupin (Lupinus angustifolius) kernels. *Journal of the Science of Food and Agriculture, 93*(15), 3755–3762.
Yang, J., Faber, I., Berton-Carabin, C. C., Nikiforidis, C. V., van der Linden, E., & Sagis, L. M. (2021). Foams and air-water interfaces stabilised by mildly purified rapeseed proteins after defatting. *Food Hydrocolloids, 112*, Article 106270.
Yang, J., Gimenez-Ribes, G., He, Q., Habibi, M., & Sagis, L. M. C. (2023). Surface dilatational and foaming properties of whey protein and escin mixtures. *Food Hydrocolloids, 144*, 108941.
Yang, J., Liu, G., Zeng, H., & Chen, L. (2018). Effects of high pressure homogenization on faba bean protein aggregation in relation to solubility and interfacial properties. *Food Hydrocolloids, 83*, 275–286.
Zudaire, E., Gambardella, L., Kurcz, C., & Vermeren, S. (2011). A computational tool for quantitative analysis of vascular networks. *PLoS One, 6*(11), Article e27385.